Preprint Title	Understanding the Role of Active Site Residues in CotB2 Catalysis Using a Cluster Model
Authors	Keren Raz, Ronja Driller, Thomas Brück, Bernhard Loll and Dan Thomas Major
Publication Date	26 Sep 2019
Article Type	Full Research Paper
Supporting Information File 1	Cartesian Coordinates for All Species.txt; 154.0 KB
ORCID® iDs	Ronja Driller - https://orcid.org/0000-0001-8834-9087; Bernhard Loll - https://orcid.org/0000-0001-7928-4488; Dan Thomas Major - https://orcid.org/0000-0002-9231-0676

Understanding the Role of Active Site Residues in CotB2 Catalysis Using a Cluster Model

Keren Raz[1], Ronja Driller[3,4,5], Thomas Brück[2], and Bernhard Loll[3], and Dan Thomas Major*[1]

[1] Department of Chemistry, Bar-Ilan University, Ramat-Gan 52900, Israel

[2] Werner Siemens Chair of Synthetic Biotechnology, Dept. of Chemistry, Technical University of Munich (TUM), Lichtenbergstr. 4, 85748 Garching, Germany

[3] Institute of Chemistry and Biochemistry, Laboratory of Structural Biochemistry, Freie Universität Berlin, Takustr. 6, 14195 Berlin, Germany

Present address:

[4] Department of Molecular Biology and Genetics, Aarhus University, Gustav Wieds Vej 10, 8000 Aarhus C, Denmark

[5] Danish Research Institute of Translational Neuroscience - DANDRITE, Nordic-EMBL Partnership for Molecular Medicine, Aarhus C, Denmark

Corresponding Author
*Dan T. Major (*majort@biu.ac.il*)

Abstract

Terpene cyclases are responsible for the initial cyclization cascade in the multistep synthesis of a large number of terpenes. CotB2 is a diterpene cyclase from Streptomyces *melanosporofaciens,* which synthesizes the formation of cyclooctat-9-en-7-ol, a precursor to the next-generation anti-inflammatory drug, cyclooctatin. In this work, we present evidence for a significant role of the active site residues in CotB2 on the reaction energetics using quantum mechanics calculations in an active site cluster model. The results using the active site model reveal the significant effect of the active site residues on the relative electronic energy of the intermediates and transition state (TS) structures with respect to gas phase data. A detailed understanding of the role of the enzyme environment on the CotB2 reaction cascade can provide important

information towards a biosynthetic strategy for cyclooctatin and the biomanufacturing of related terpene structures.

Keywords

Diterpene; quantum mechanics; CotB2 cyclase; mechanism; active site

Introduction

Enzymes catalyze numerous, complex bio-chemical reactions in different cellular compartments. .[1] More specifically, the enigmatic class of terpene cyclases is responsible for converting linear, aliphatic oligoprenyldiphosphates into various, chemically complex macrocyclic products. The resulting terpene scaffolds and their functionalized terpenoid analogues, comprise the largest and structurally most diverse family of natural products, currently representing over 50,000 reported structures from all kingdoms of life.[2] The largest diversity of terpenoids is reported for the plant kingdom, where terpenes as secondary metabolic products, are responsible for, e.g. defense against biotic and abiotic stress or attracting insects for pollination.[3, 4] Industrially, terpene type natural products are employed as flavoring agents [5], fragrances, spices, cosmetics, perfume, biofuel, and in agriculture.[4] Additionally, terpene type natural products with numerous pharmacological [6] and biological activities have been reported, rendering them important targets for medical and biotechnology research.[7] Chemical synthesis and sustainable biosynthesis strategies in synergy with the biological activity of different terpene type natural products, have been investigated in detail.[8, 9, 10]

The first crystal structure of a monoterpene cyclase [11] was reported in 2002. Subsequently, the first crystal structure of a sesquiterpene [12] and a triterpene [13] cyclase were published in 1997. Less than a decade ago, the first crystal structure of a diterpene cyclase was reported by Christianson and co-workers.[14] These structures, in conjunction with extensive biochemical work,[8, 15] have contributed to the understanding of the mechanistic details of terpene cyclases, and facilitate rational enzyme design[16]. Theoretical quantum mechanical (QM) investigations on the chemistry of terpenes in the gas-phase have provided detailed understanding of the carbocation mechanisms underlying terpene synthase function.[17, 18] Further, Major and co-workers have used multiscale modelling tools to study the effect of the enzyme environment in catalyzing reactions in mono-, sesqui-, and di-terpene synthases.[19]

Diterpenes are generated from the universal aliphatic substrate geranyl geranyl pyrophosphate (GGPP).[3] In-vitro experiments demonstrated that many diterpenes have pharmaceutical applications by featuring anticancer, antibacterial, anti-

inflammatory and antiretroviral activities[20]. Moreover, they can be applied in the food industry as antioxidants and sweeteners.[3]

CotB2 is a bacterial diterpene cyclase from Streptomyces *melanosporofaciens,* which synthesizes the formation of cyclooctat-9-en-7-ol, representing the first committed step in the biosynthesis of the next-generation anti-inflammatory drug to cyclooctatin. The intracellular target of cyclooctatin is a, as yet uncharacterized lysophospholipase, which is involved in early steps of the inflammatory signaling cascade.[21-23] In the last decade numerous interdisciplinary studies have addressed the chemical mechanism of CotB2 catalysis utilizing different detection and analysis methods.

Meguro et al. [24] established the chemical mechanism for formation of cyclooctatin using isotope labeling experiments (Scheme 1). Recently, Hong and Tantillo [21] and Sato et al. [22] investigated the CotB2 mechanism using QM tools. According to Meguro et al., [24] the cyclization process commences with dissociation of the pyrophosphate leaving group of GGPP, forming an allylic carbocation and, two subsequent electrophilic cyclizations generate intermediate **A**. Intermediate **A** undergoes a 1,5-hydride shift, forming intermediate **B**. A subsequent cyclization forms intermediate **C**. Intermediate **C** generates intermediate **E**, via one of two possible pathways: either a direct 1,3-hydrid shift, or an indirect pathway, involving two 1,2-hydride shifts. Theoretical investigations by Hong and Tantillo suggested that the indirect transformation from intermediate **C** to **E** is energetically favored and might be biosynthetically relevant.[21] This finding is in agreement with Sato et al.[22] who performed isotope labeling experiments combined with QM calculations. Intermediate **G** forms via a 1,5-hydride shift from C6 to C10 to generate a homoallylic cation, and the formation of intermediate **H** occurs due to cyclization to yield a cyclopropyl ring. Intermediate **I** forms due to isomeric formation of a cyclopropylcarbinyl cation, as shown by isotope labeling.[24] QM calculations support this unusual 1,3 alkyl shift that interconverts **H** and **I**.[21, 22] Finally, the cyclopropyl ring opens by virtue of a nucleophilic water attack and cyclooctat-9-en-7-ol is formed.

Although gas phase calculations shed light on the reactivity of the isolated species and provide crucial mechanistic insight, the bio-relevant mechanism cannot be fully understood without taking into account the enzyme-solvent environment. A common problem when studying these enzymes is the lack of high-resolution crystal structures, that are biologically relevant, i.e. have a ligand bound in a reactive

configuration and have a fully closed active site. Recently, a crystal structure of the CotB2 enzyme that meets these criteria became available.[25] In the current work we describe the crucial role of the amino acids in the active site on the reaction energetics using QM calculations in an active site cluster model. The results obtained using the active site model are compared with gas-phase data.

Results and Discussion

The energy profiles for both gas phase (orange) and for the active site model (blue) reactions are characterized by a sequential decreasing pattern (Fig. 1). Inspection of the gas-phase profile reveals important information regarding the inherent reactivity [18] of the carbocation species. As the reaction proceeds, π-bonds transform into σ-bonds, explaining the steady downhill progress of the energy profile. An additional general feature is the relatively low energy barriers separating the intermediates that are less than ca. 10 kcal/mol. The gas-phase mechanism has been discussed extensively by Hong and Tantillo[21] and Sato et al.[22] Here we focus on the difference between the gas-phase and active site model energies. All interaction distances are provided in Table 1.

Carbocation **A** is stabilized through π-cation interaction with W186, while **B** is stabilized due to dipole-cation interactions of the allylic carbocation formed on C6-C7-C8, with N103, T106, and I181. These variations in interactions result in an energy difference of 14.2 kcal/mol favoring **B**, and the barrier is reduced by 2.8 kcal/mol (Fig. 1). Another possible reason for stabilization is that C7 has a greater proximity to the pyrophosphate group than C15 (6.71 Å vs. 7.54 Å, Table 1, Fig. 2). The energy difference between **B** and **C** is 15.7 kcal/mol in the active site model, compared to 8.7 kcal/mol in the gas-phase. Here the energy gain is likely due to the fact that the carbocation in intermediate **C** is located 4.21 Å from the pyrophosphate group, which stabilizes it (Table 1, Fig. 2). Moreover, π-cation interactions with F107 contributes to the stabilization as well. The activation energy for the formation of **C** is 2.4 kcal/mol in the active site model compared to 4.3 kcal/mol in the gas phase. In the active site model, **D** is less stable than **C** by almost 2 kcal/mol, while in the gas-phase **D** is more stable by ca. 2 kcal/mol. The main reason for this difference is possibly a difference in the conformation of **D** in the active site model compared to the gas phase. The dihedral angle C3-C2-C6-C7 in **D** is greater by 53º in the active site model than in the gas

phase, and the D dihedral angle C10-C9-C8-C7 in the active site is smaller by 258º than in the gas phase (Fig. 3). Moreover, the dihedral angle C2-C1-C11-C10 is greater by 281º in the active site model. The distance between C4 and C13 is significantly greater in the active site model (1.2 Å), indicating a more extended conformation. Figure 4A shows clearly that intermediate **D** is more folded in the gas phase than in the active site model. The required activation energy to form **D** is 4.1 kcal/mol lower in the active site model than the gas phase, likely due to π-cation interactions with F107 and F149 and greater proximity to the negatively charged pyrophosphate group. Another conformational difference between gas-phase and in the enzyme model appears in **E** as well (Fig. 4B). The dihedral angle C2-C3-C4-C5 is greater by 285º and C10-C9-C8-C7 is smaller by 294º in the active site model than the gas phase. Moreover, the angle C2-C1-C11 is greater by 5º in the active site model than in the gas phase, and the distance between C4 and C13 is smaller by 0.5 Å in the gas phase. The net result of these differences is that intermediate **E** is more folded in the gas phase, although, it is not as dramatically folded as **D**. The reason for greater folding in the gas phase could be a tendency to adopt conformations which maximizes intramolecular dispersion interactions. In the active site model of **E**, the carbocation on C6 is at a greater distance from the pyrophosphate group than C2 in cation **D** (6.03 Å vs. 5.03 Å) and likely contributes to a slight destabilizing effect of the active site model. This is in spite of interactions between cation **D** and N103, T106, F107, and F149. Nonetheless, the energy barrier to form **E** is higher in the active site model than in the gas-phase. An elevated energy barrier is also observed for formation of **G** (by almost 10 kcal/mol). This may be explained by loss of interaction between **G** and the pyrophosphate moiety, as the cation moves away, deeper into the hydrophobic part of the pocket. A distinct carbocation **G** is not observed in the enzyme model. Instead, a cation resembling **H**, with a C8-C10 bond that is already partly formed is observed. This carbocation is more stable in the active site model than **G** in the gas phase by almost 9 kcal/mol. Hence, in the enzyme model, cation **G** is not a stable species, and instead **H** is formed spontaneously. The energy for transformation **E** to **H** is very similar in the gas-phase and in the enzyme. Carbocation **H** forms interactions with N103, W186, and especially with I181. The relative energy difference between **H** and **I** is also similar in the gas-phase and in the enzyme model. However, the activation energy is higher by 3.0 kcal/mol in the active site model, possibly due to steric effects. **I** is

stabilized via interactions with N103, I181, and W186, which likely make similar stabilizing contributions as in cation **H**.

It is well established that the inherent reactivity of carbocations,[18] as well as correct substrate folding in the active site,[10] play crucial roles in terpene synthases. The current results highlight the importance of taking into account the active site residues while modelling terpene synthase mechanisms, as we have proposed previously.[19, 25] We find that the energy surface in the active site model is significantly perturbed compared to the gas phase potential. Additionally, structural analysis reveals that each cation is stabilized by non-covalent interactions, like ionic, π-cation and dipole-cation interactions. These findings suggest that rational biosynthesis of novel terpenes might be possible by careful design of CotB2 mutants. Future studies using multiscale techniques to model the enzyme reaction in a complete enzyme environment will allow careful evaluation of the usefulness of such active site models.

Scheme 1: Mechanism for formation of cyclooctat-9-en-7-ol.

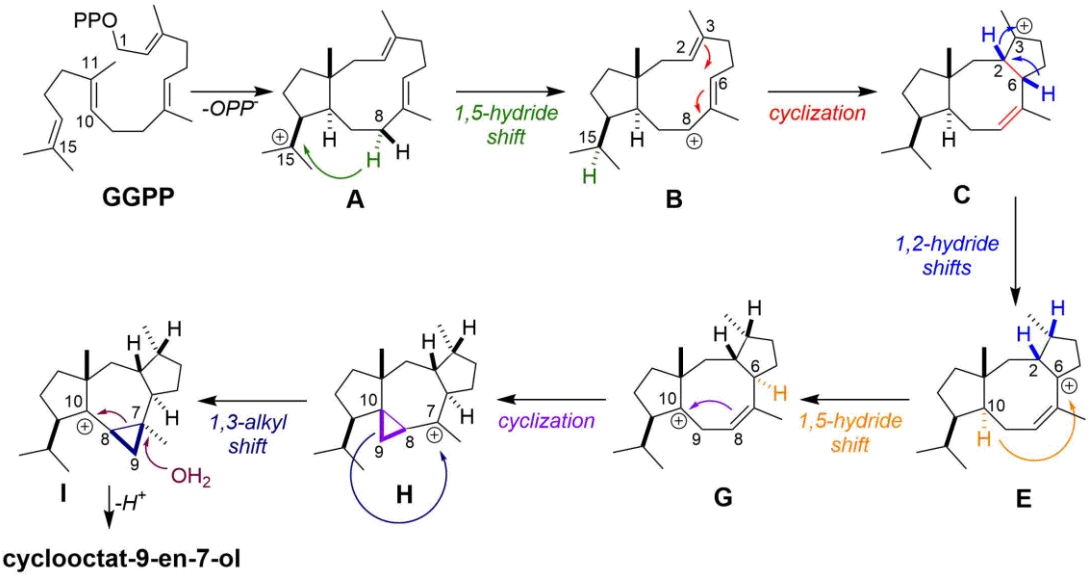

Figure 1: Computed electronic energy profiles (kcal/mol) for the CotB2 cyclase mechanism. The calculations used M062X/6-31+G(d,p).

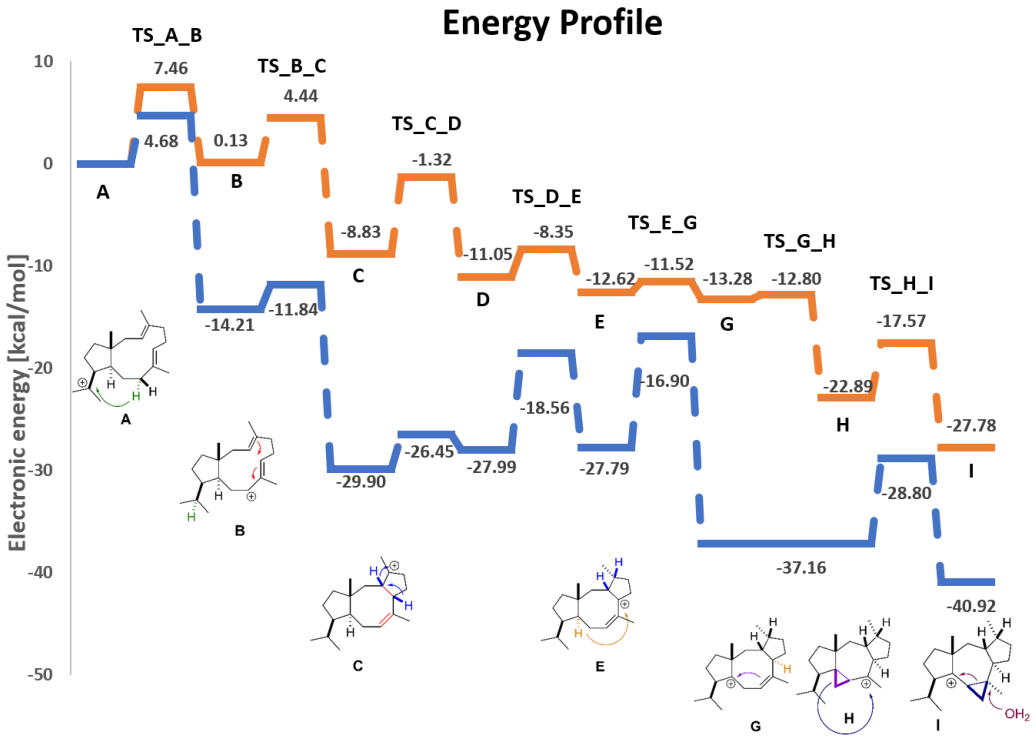

Table 1: Interactions between intermediates and TS structures with active site residues.

Intermediate	Interacting species		Distance (Å)	Interaction type
A	W186	C_{15}	4.49	π-cation
	I181	C_{15}	3.80	Dipole-cation
B	N103	C_6	4.66	Dipole–cation (C=O)
	N103	C_7	4.72	Dipole–cation (C=O)
	N103	C_8	4.41	Dipole–cation (C=O)
	T106	C_6	3.96	Dipole–cation (OH)
	T106	C_7	4.15	Dipole–cation (OH)
	T106	C_8	5.33	Dipole–cation (OH)
	F107	C_6	4.25	π–cation
	F107	C_7	5.53	π–cation
	F107	C_8	5.88	π–cation
	I181	C_6	5.15	Dipole–cation
	I181	C_7	4.45	Dipole–cation
	I181	C_8	4.14	Dipole–cation
C	O_3	C_3	4.20	Anion–cation
	F107	C_3	3.65	π–cation
	I181	C_3	4.72	Dipole–cation
D	O_3	C_2	5.03	Anion–cation
	F107	C_2	4.35	π–cation
E	N103	C_6	4.74	Dipole–cation (C=O)
	N103	C_7	3.81	Dipole–cation (C=O)
	N103	C_8	3.04	Dipole–cation (C=O)
	T106	C_6	4.43	Dipole–cation (OH)
	T106	C_7	4.25	Dipole–cation (OH)
	T106	C_8	5.32	Dipole–cation (OH)
	F107	C_6	4.66	π–cation
	F107	C_7	5.37	π–cation
	F107	C_8	5.54	π–cation
	F149	C_6	5.84	π–cation
	F149	C_7	6.42	π–cation
	F149	C_8	7.75	π-cation
G/H	N103	C_7	5.91	Dipole–cation
	T106	C_7	5.27	Dipole–cation (OH)
	F149	C_7	5.35	π–cation
	I181	C_7	3.08	Dipole–cation (C=O)
	W186	C_7	6.48	π–cation
I	N103	C_{10}	5.44	Dipole–cation
	I181	C_{10}	3.31	Dipole–cation (C=O)
	W186	C_{10}	5.87	π–cation

TS structure	Interaction species		Distance Å	Interaction type
A_B	I181	C_{15}	3.85	Dipole–cation
	I181	C_8	4.80	Dipole–cation
	W186	C_{15}	4.48	π–cation
	W186	C_8	5.09	π–cation
B_C	O_3	C_2	3.78	
	O_3	C_6	5.88	Anion–cation
	N103	C_2	6.26	
	N103	C_6	4.80	Dipole–cation (C=O)
	T106	C_2	6.80	
	T106	C_6	4.30	Dipole–cation (OH)
	F107	C_2	4.12	
	F107	C_6	4.36	π–cation
	I181	C_2	4.33	
	I181	C_6	4.80	Dipole–cation
C_D	O_3	C_2	4.88	Anion–cation
	O_3	C_3	4.39	Anion–cation
	F107	C_2	4.42	π–cation
	F107	C_3	3.61	π–cation
	I181	C_2	4.00	Dipole–cation
	I181	C_3	4.85	Dipole–cation
D_E	O_3	C_2	4.66	Anion–cation
	O_3	C_6	5.82	Anion–cation
	F107	C_2	4.55	π–cation
	F107	C_6	5.37	π–cation
	F149	C_2	5.93	π–cation
	F149	C_6	5.05	π–cation
E_G/H	N103	C_6	6.09	Dipole–cation (C=O)
	N103	C_{10}	5.20	Dipole–cation (C=O)
	F107	C_6	5.07	π–cation
	F107	C_{10}	5.15	π–cation
	F149	C_6	5.42	π–cation
	I181	C_6	3.62	Dipole–cation (OH)
	I181	C_{10}	3.84	Dipole–cation (OH)
G/H_I	N103	C_7	5.41	Dipole–cation
	N103	C_{10}	5.81	Dipole–cation
	T106	C_7	5.11	Dipole–cation (OH)
	T106	C_{10}	7.29	Dipole–cation (OH)
	F149	C_7	5.68	π–cation
	F149	C_{10}	7.76	π–cation
	I181	C_7	3.47	Dipole–cation (C=O)
	I181	C_{10}	3.03	Dipole–cation (C=O)
	W186	C_7	6.09	π–cation
	W186	C_{10}	5.70	π–cation

Figure 2: Intermediates **A-I** in the active site model. Interactions are marked by dashed orange line, the interacting residues are labeled in black, the non-interacting residues are labeled in dark grey, and plus signs note location of the cation.

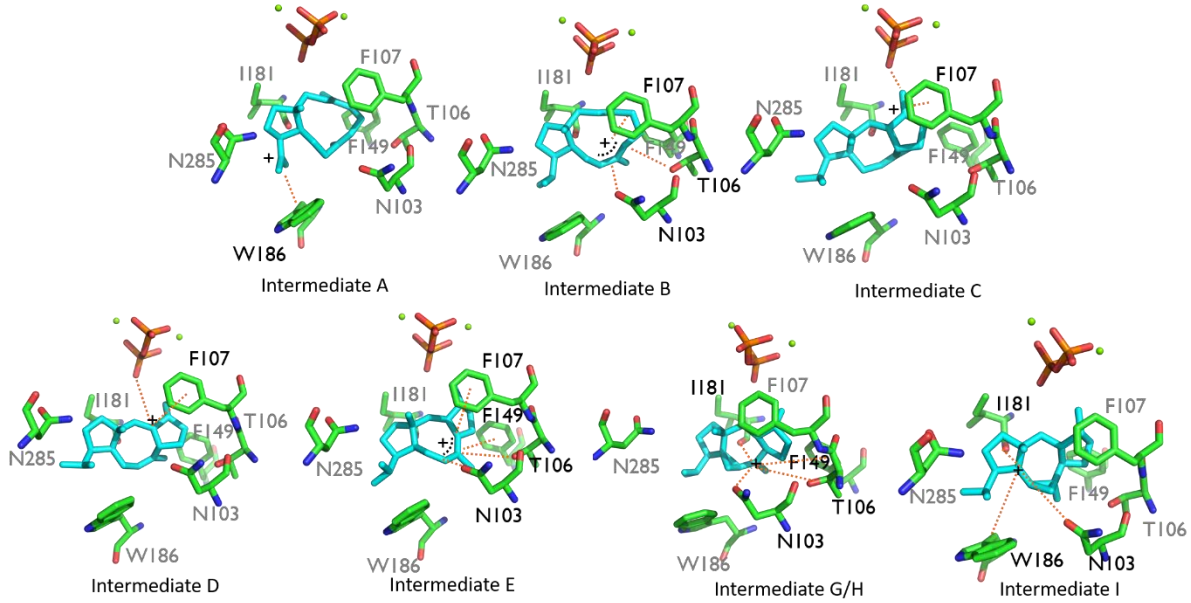

Figure 3: TS structures TS_**A_B**-TS_**G/H_I** in the active site model. Interactions are marked by dashed orange lines, the interacting residues are labeled in black, the non-interacting residues are labeled in dark grey, and the plus signs note the location of the cation.

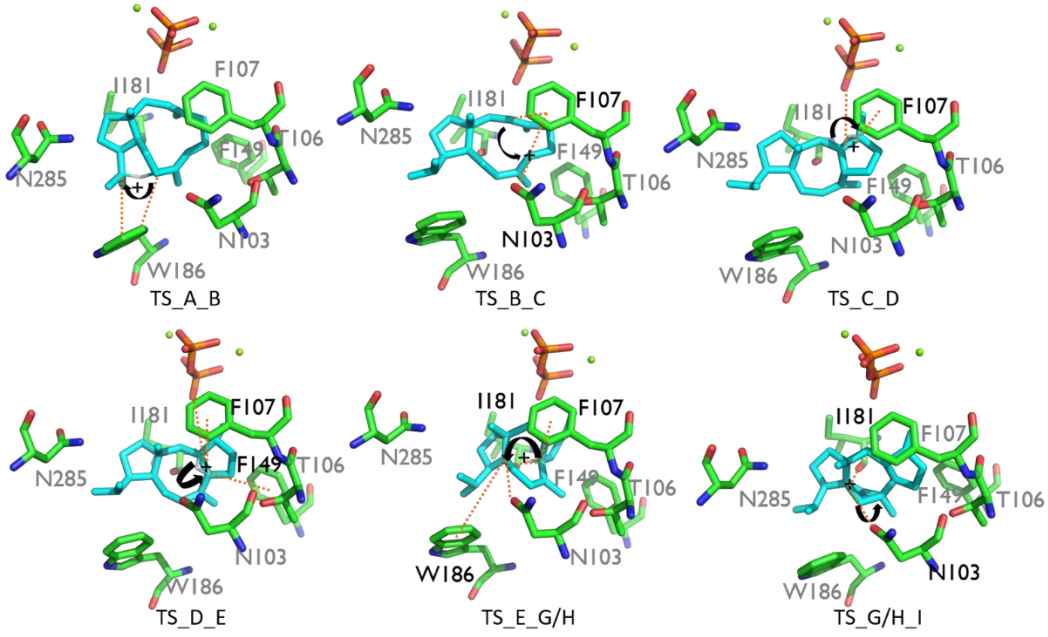

Figure 4: Comparison between gas phase and active site model conformations. A) Intermediate **D**. B) Intermediate **E**.

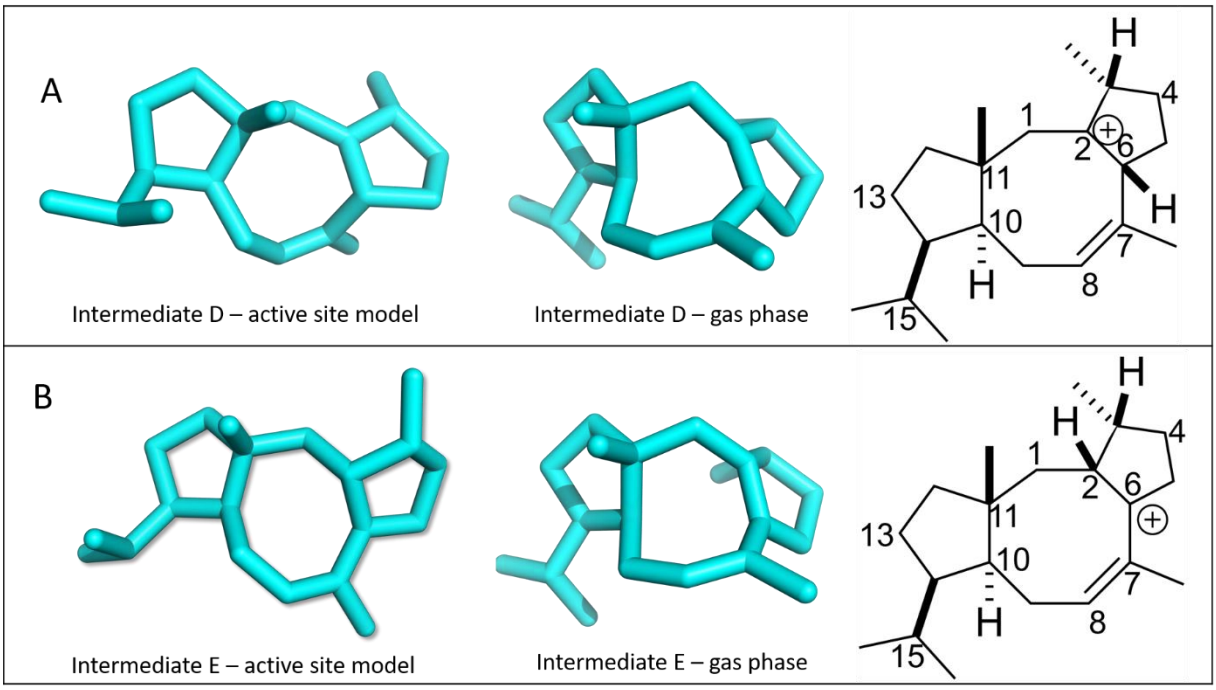

Table 2: Comparison table of transition state structures in gas phase vs. active site model

			Gas phase	Active site model
TS structure	Interaction species		Distance Å	Distance Å
TS_**A_B**	C_{15}	H_{82}	1.21	1.29
	C_8	H_{82}	1.46	1.34
	C_8	C_{15}	2.58	2.52
TS_**B_C**	C_2	C_6	2.44	2.61
TS_**C_D**	C_2	H_2	1.21	1.44
	C_3	H_2	1.48	1.24

	C_3	C_2	1.41	1.41
TS_**D_E**	C_6	H_6	1.25	1.38
	C_2	H_6	1.41	1.28
	C_2	C_6	1.41	1.42
TS_**E_G/H**	C_6	H_6	1.12	1.14
	C_{10}	H_6	1.74	1.63
	C_{10}	C_6	2.63	2.49
	C_8	C_{10}	2.33	2.54
TS_**H_I**	C_9	C_7	1.71	1.66
	C_9	C_{10}	1.65	1.69
	C_{10}	C_7	2.48	2.46

Conclusion

In this work, we compared the energy profiles of the terpene cyclase CotB2 reaction obtained in the gas phase and using an active site model. The calculations used identical QM methods, facilitating a direct comparison. We presented evidence for an important role played by the active site residues in CotB2 on the reaction energetics in an active site cluster model, suggesting that reaction control in terpene synthase is obtained via a combination of inherent reactivity, initial substrate folding and enzyme environmental effects. Specifically, the results using the active site model reveal the significant effect the active site residues have on the relative electronic energy of the intermediates and TS structures in comparison with gas phase data, due to ionic, π-cation and dipole-cation interactions. A detailed understanding of the role of the enzyme environment on the reaction cascade in CotB2 can provide important information towards a synthetic strategy for cyclooctatin and related terpene manufacturing. Future studies using hybrid quantum mechanics and molecular mechanics techniques to model the enzyme reaction in a complete enzyme environment will allow careful evaluation of the usefulness of such active site models.

Experimental

All calculations were carried out with Gaussian 16.[26] Geometry optimizations, frequency calculations and intrinsic coordinate calculations were performed using the M062X/6-31+G(d,p) level of theory.[27] The gas phase structures were taken from Sato et al.[22] The amino-acid cage was constructed from 6 amino acids, which are located around the substrate and constitute part of the catalytic pocket of the enzyme (PDB-ID 6GGI)[25]. The chosen amino acids are the ones that we presume stabilize the carbocations the most during the reaction. The coordinates of the amino-acids and the substrate GGPP were taken from the X-ray structure with resolution of 1.8 Å.[25] In this approach, geometry optimizations with the “Modredundant” keyword were performed, and the active site residues, diphosphate moiety and magnesium ions are fixed throughout the reaction progress. The entire cage system is treated using the above mentioned DFT method. In order to find the TS structures, complete TS optimizations using the keywords QST2, QST3 and “Modredundant” were performed. The Cartesian coordinates of all species are reported in the Supporting Information.

Supporting Information

File Name: Cartesian Coordinates for All Species

File Format: txt file

Acknowledgements

This work was supported by the Israeli Science Foundation (Grants # 1683/18).

References

1. Knowles, J. R. *Nature* **1991**, *350* (6314), 121; Warshel, A. *Proc. Natl. Acad. Sci. U.S.A.* **1978**, *75* (11), 5250-5254.
2. Greenhagen, B.; Chappell, J. *Proc. Natl. Acad. Sci. U.S.A.* **2001**, *98* (24), 13479-13481.
3. Devappa, R. K.; Makkar, H. P.; Becker, K. *J. Am. Oil Chem.' Soc.* **2011**, *88* (3), 301-322.
4. Singh, B.; Sharma, R. A. *3 Biotech* **2015**, *5* (2), 129-151.
5. Schwab, W.; Davidovich-Rikanati, R.; Lewinsohn, E. *Plant J.* **2008**, *54* (4), 712-732.
6. Dewick, P. M. *Medicinal natural products: a biosynthetic approach*; John Wiley & Sons: 2002; Radhakrishna, S.
7. Rates, S. M. K. *Toxicon* **2001**, *39* (5), 603-613.
8. Gershenzon, J.; Dudareva, N. *Nat. Chem. Biol.* **2007**, *3* (7), 408; Cane, D. E. *Chem. Rev.* **1990**, *90* (7), 1089-1103; Christianson, D. W. *Chem. Rev.* **2006**, *106* (8), 3412-3442.
9. Gonzalez-Burgos, E.; Gomez-Serranillos, M. *Curr. Med. Chem.* **2012**, *19* (31), 5319-5341; *ACS symposium series*, 1995; Tholl, D. *Curr. Opin. Plant Biol.* **2006**, *9* (3), 297-304; Zwenger, S.; Basu, C. *Biotechnol. Mol. Biol. Rev.* **2008**, *3* (1), 1; Janke, R.; Görner, C.; Hirte, M.; Brück, T.; Loll, B. *Acta Crystallogr. D* **2014**, *70* (6), 1528-1537.
10. Christianson, D. W. *Chem. Rev.* **2017**, *117* (17), 11570-11648.
11. Whittington, D. A.; Wise, M. L.; Urbansky, M.; Coates, R. M.; Croteau, R. B.; Christianson, D. W. *Proc. Natl. Acad. Sci. U.S.A.* **2002**, *99* (24), 15375-15380.
12. Lesburg, C. A.; Zhai, G.; Cane, D. E.; Christianson, D. W. *Science* **1997**, *277* (5333), 1820-1824; Starks, C. M.; Back, K.; Chappell, J.; Noel, J. P. *Science* **1997**, *277* (5333), 1815-1820.
13. Wendt, K. U.; Poralla, K.; Schulz, G. E. *Science* **1997**, *277* (5333), 1811-1815.
14. Köksal, M.; Jin, Y.; Coates, R. M.; Croteau, R.; Christianson, D. W. *Nature* **2011**, *469* (7328), 116.
15. Croteau, R. *Chem. Rev.* **1987**, *87* (5), 929-954.
16. Brück, T.; Kourist, R.; Loll, B. *ChemCatChem* **2014**, *6* (5), 1142-1165.
17. Tantillo, D. J. *Nat. Prod. Rep.* **2011**, *28* (6), 1035-1053; Hess Jr, B. A.; Smentek, L.; Noel, J. P.; O'Maille, P. E. *J. Am. Chem. Soc.* **2011**, *133* (32), 12632-12641.
18. Tantillo, D. J. *Angew. Chem.* **2017**, *56* (34), 10040-10045.
19. Dixit, M.; Weitman, M.; Gao, J.; Major, D. T. *ACS Catal.* **2016**, *7* (1), 812-818; Weitman, M.; Major, D. T. *J. Am. Chem. Soc.* **2010**, *132* (18), 6349-6360; Major, D. T.; Weitman, M. *J. Am. Chem. Soc.* **2012**, *134* (47), 19454-19462; Gao, J.; Ma, S.; Major, D. T.; Nam, K.; Pu, J.; Truhlar, D. G. *Chem. Rev.* **2006**, *106* (8), 3188-3209; Major, D. T.; Freud, Y.; Weitman, M. *Curr. Opin. Chem. Biol.* **2014**, *21*, 25-33; Ansbacher, T.; Freud, Y.; Major, D. T. *Biochemistry* **2018**, *57*, 3773-3779; Dixit, M.; Weitman, M.; Gao, J.; Major, D. T. *ACS Catal.* **2017**, *7*, 812-818; Freud, Y.; Ansbacher, T.; Major, D. T. *ACS Catal.* **2017**, *7*, 7653-7657; Major, D. T. *ACS Catal.* **2017**, *7*, 5461-5465.
20. Newman, D. J.; Cragg, G. M. *J. Nat. Prod.* **2016**, *79* (3), 629-661.
21. Hong, Y. J.; Tantillo, D. J. *Org. Biomol. Chem.* **2015**, *13* (41), 10273-10278.

22. Sato, H.; Teramoto, K.; Masumoto, Y.; Tezuka, N.; Sakai, K.; Ueda, S.; Totsuka, Y.; Shinada, T.; Nishiyama, M.; Wang, C. *Sci. Rep.* **2015**, *5*, 18471.
23. Kim, S.-Y.; Zhao, P.; Igarashi, M.; Sawa, R.; Tomita, T.; Nishiyama, M.; Kuzuyama, T. *Chem. Biol.* **2009**, *16* (7), 736-743.
24. Meguro, A.; Motoyoshi, Y.; Teramoto, K.; Ueda, S.; Totsuka, Y.; Ando, Y.; Tomita, T.; Kim, S. Y.; Kimura, T.; Igarashi, M. *Angew. Chem.* **2015**, *54* (14), 4353-4356.
25. Driller, R.; Janke, S.; Fuchs, M.; Warner, E.; Mhashal, A. R.; Major, D. T.; Christmann, M.; Brück, T.; Loll, B. *Nat. Commun.* **2018**, *9* (1), 3971.
26. Frisch, M. J.; Trucks, G. W.; Schlegel, H. B.; Scuseria, G. E.; Robb, M. A.; Cheeseman, J. R.; Scalmani, G.; Barone, V.; Petersson, G. A.; Nakatsuji, H.; Li, X.; Caricato, M.; Marenich, A. V.; Bloino, J.; Janesko, B. G.; Gomperts, R.; Mennucci, B.; Hratchian, H. P.; Ortiz, J. V.; Izmaylov, A. F.; Sonnenberg, J. L.; Williams; Ding, F.; Lipparini, F.; Egidi, F.; Goings, J.; Peng, B.; Petrone, A.; Henderson, T.; Ranasinghe, D.; Zakrzewski, V. G.; Gao, J.; Rega, N.; Zheng, G.; Liang, W.; Hada, M.; Ehara, M.; Toyota, K.; Fukuda, R.; Hasegawa, J.; Ishida, M.; Nakajima, T.; Honda, Y.; Kitao, O.; Nakai, H.; Vreven, T.; Throssell, K.; Montgomery Jr., J. A.; Peralta, J. E.; Ogliaro, F.; Bearpark, M. J.; Heyd, J. J.; Brothers, E. N.; Kudin, K. N.; Staroverov, V. N.; Keith, T. A.; Kobayashi, R.; Normand, J.; Raghavachari, K.; Rendell, A. P.; Burant, J. C.; Iyengar, S. S.; Tomasi, J.; Cossi, M.; Millam, J. M.; Klene, M.; Adamo, C.; Cammi, R.; Ochterski, J. W.; Martin, R. L.; Morokuma, K.; Farkas, O.; Foresman, J. B.; Fox, D. J. *Gaussian 16, Revision A. 03*, Wallingford, CT, 2016.
27. Zhao, Y.; Truhlar, D. G. *Theor. Chem. Acc.* **2008**, *120* (1-3), 215-241.